ac response of bipolar double-barrier resonant-tunneling structures

A. Kindlihagen
Department of Physics and Measurement Technology, University of Linköping, S-58183 Linköping, Sweden

A. G. Mal'shukov
Institute of Spectroscopy, Russian Academy of Science, 142092, Troitsk, Moscow Region, Russia

K. A. Chao
Department of Theoretical Physics, Lund University, S-22362 Lund, Sweden

M. Willander
Physical Electronics and Photonics, Department of Physics, Chalmers University of Technology, S-41296 Göteborg, Sweden
(Received 30 September 1997)

We have developed an explicit formulation of the total intrinsic admittance of bipolar double-barrier resonant-tunneling structures. The theory includes contributions from the tunneling currents through the barriers and the recombination current, as well as from the charge distribution. We have numerically solved the problem for small ac voltage amplitudes in the framework of linear response. The calculations are fully quantum mechanical in the Hartree approximation. In linear response, and at frequencies below the internal frequency of the system, the susceptance is found to be entirely of a capacitive nature. We have studied both an ordinary bipolar double-barrier resonant-tunneling structure and an optimized resonant-tunneling light emitting diode. We have investigated the frequency dependence of the admittance as well as the dependence on recombination time. In both samples a δ-shaped peak in the susceptance is found in the negative differential resistance region. However, the details of the frequency response are found to be closely related to the specific structure under consideration. [S0163-1829(98)04739-0]

I. INTRODUCTION

Resonant tunneling (RT) is a phenomenon utilized in a variety of electronic devices. Especially the *double-barrier resonant-tunneling structures* (DBRTS's) are much used for technological applications. The unipolar DBRTS is, for instance, used for RT diodes, RT oscillators, switches, and bistable lasers. The bipolar DBRTS has been proposed for applications, such as the RT light emitting diode (LED).[1–4] Apart from its technological applications, the DBRTS is also a nanostructure of rich quantum phenomena, and thus very interesting for fundamental theoretical research.

In resonant tunneling the *current-voltage (I-V)* measurement and the *capacitance-voltage (C-V)* measurement are of basic importance. The unipolar DBRTS has been a very popular system for experimental and theoretical studies of both the *I-V* and the *C-V* characteristics of resonant tunneling. The dc *I-V* characteristics are thoroughly investigated and well understood, while both the *C-V* characteristics and the inductive behavior are still under discussion. The *C-V* characteristics of RT structures are generally strongly nonlinear and show clear fingerprints of the quantum confinement, the so-called *quantum capacitance*. The quantum capacitance was first recognized by Luryi,[5] and has been investigated in various structures with quantum confinement,[6–10] including the unipolar DBRTS.[5,11–14] Some work on the inductance of the unipolar DBRTS has also been presented,[15,16] as well as general treatments of admittance.[17–22]

The bipolar DBRTS is a much less studied system, on which very little theoretical work has been performed. Only recently we presented the first thorough theoretical investigation of the steady state properties of the bipolar DBRTS,[4] and to our knowledge there exists no theoretical work at all on the ac properties of this structure.

The problem in calculating the ac response of RT systems is that for semitransparent barriers one cannot unambiguously split the system into isolated regions in order to substitute the charge stored there into the conventional definition of the capacitance $C=dQ/dV$. Therefore, we employ a more explicit approach based on an analysis of the frequency dependence of the current across the whole system. We will consider the case when the electron and hole relaxation rate in the quantum well is larger than both the ac frequency and the tunneling and recombination rates. The electrons and holes inside the quantum well can then be described by a quasiequilibrium state. This has allowed us to write a closed differential equation for the time dependence of the charge stored in the well. In linear response the parameters of this equation will be calculated from a self-consistent steady state solution of the system. After the charge inside the well is found we can determine the current across the system and thus the complex admittance Y of the DBRTS. Its textbook definition is given by $I(t)=YV(t)$. The current $I(t)$ can be separated into one part *in phase* with the applied voltage I^{IP} and one part *out of phase*, I^{OP}. I^{IP} corresponds to $\mathrm{Re}(Y)$ and represents the conductance G, while I^{OP}, which is 90° out of phase with the applied voltage, corresponds to $\mathrm{Im}(Y)$. The imaginary part, or the susceptance B, consists of the capacitance C and the inductance L, both contributing to B with

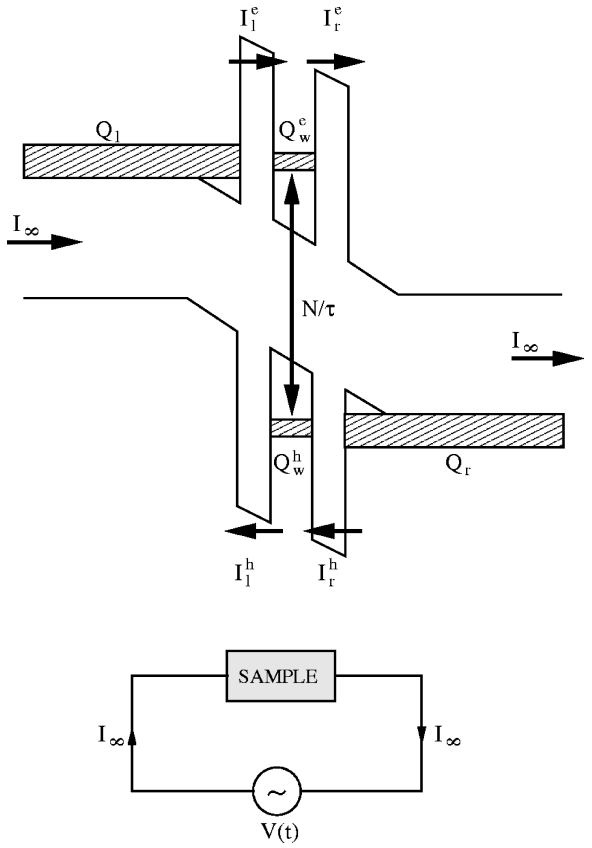

FIG. 1. Schematic sketch of the bipolar DBRTS (upper part) and a principal sketch of the ac circuit (lower part).

their specific frequency dependencies. Consequently, one can find C and L from the shape of the $B(\omega)$ curve.

This approach is a generalization of our previous work on a unipolar DBRTS.[17] However, for a bipolar DBRTS we have to take into account the tunneling currents of both electrons and holes, as well as the electron-hole recombination process. This accounts for an extremely complicated analysis for steady-state calculations, and certainly even more for investigation of ac properties.

The paper is organized as follows. In Sec. II we define the system under consideration and develop the theoretical model. The theory is employed for numerical studies of two different samples in Sec. III. Finally we give some comments in Sec. IV.

II. THEORY

A. Quantum admittance

Our system is schematically illustrated in Fig. 1. The *sample* in the circuit is the DBRTS. In order to be consistent with our earlier work on the bipolar DBRTS (Ref. 4) and our work on the admittance of the unipolar DBRTS (Ref. 17) we use the following conventions. The electron tunneling currents, I_l^e and I_r^e, and the current in the contacts, I_∞, are defined positive for an electron tunneling from left to right, while the hole tunneling currents, I_l^h and I_r^h, are defined positive for a hole tunneling from right to left. All charges, including the hole charge in the quantum well Q_w^h, are treated as electronic charge.

The charge Q_l in the left reservoir, the current I_∞ in the left contact, and the electron and hole tunneling currents I_l^e and I_l^h through the left barrier then satisfy the equation

$$\frac{dQ_l}{dt} = I_\infty(t) - I_l^e(t) - I_l^h(t). \tag{1}$$

If we rewrite Eq. (1) as

$$I_\infty(t) = I_l^e(t) + I_l^h(t) + \frac{dQ_l}{dV}\frac{dV}{dt}, \tag{2}$$

making use of the general definition of admittance and assuming an ac voltage $V(t) = V \sin \omega t$ it becomes

$$I_\infty(t) = I_l^{IP,e}(t) + I_l^{IP,h}(t) + I_l^{OP,e}(t) + I_l^{OP,h}(t) + \frac{dQ_l}{dV}\frac{dV}{dt}$$
$$= \mathrm{Re}(Y) V \sin\ \omega t + \mathrm{Im}(Y) V \cos\ \omega t. \tag{3}$$

The *in-phase* part gives the conductance

$$\mathrm{Re}(Y) = G = \frac{I_l^{IP,e} + I_l^{IP,h}}{V \sin\ \omega t}, \tag{4}$$

while the *out-of-phase* components give the susceptance

$$\mathrm{Im}(Y) = B = \omega\left(\frac{I_l^{OP,e} + I_l^{OP,h}}{dV/dt} + \frac{dQ_l}{dV}\right). \tag{5}$$

We have derived the above results by analyzing the currents at the left part of the DBRTS shown in Fig. 1. However, the results should be independent of which side of the DBRTS one considers. We will therefore briefly repeat the analyses with Q_r instead of Q_l to demonstrate this fact. Analogous to (1) the charge Q_r and the currents I_r^e, I_r^h, and I_∞ satisfy

$$\frac{dQ_r}{dt} = I_r^e(t) + I_r^h(t) - I_\infty(t), \tag{6}$$

which we rewrite as

$$I_\infty(t) = I_r^{IP,e}(t) + I_r^{IP,h}(t) + I_r^{OP,e}(t) + I_r^{OP,h}(t) - \frac{dQ_r}{dV}\frac{dV}{dt}. \tag{7}$$

This give for the conductance

$$\mathrm{Re}(Y) = G = \frac{I_r^{IP,e} + I_r^{IP,h}}{V \sin\ \omega t}, \tag{8}$$

and for the susceptance

$$\mathrm{Im}(Y) = B = \omega\left(\frac{I_r^{OP,e} + I_r^{OP,h}}{dV/dt} - \frac{dQ_r}{dV}\right). \tag{9}$$

The two alternative expressions for the susceptances (5) and (9) are consistent with the conservation law

$$\frac{d}{dV}(Q_w^e + Q_w^h + Q_l + Q_r) = 0. \tag{10}$$

To prove this we rewrite Eqs. (3) and (7) as

$$I_\infty(t)-I_l^{IP,e}(t)-I_l^{IP,h}(t)=\frac{\mathrm{Im}(Y)}{\omega}\frac{dV}{dt},$$

$$I_\infty(t)-I_r^{IP,e}(t)-I_r^{IP,h}(t)=\frac{\mathrm{Im}(Y)}{\omega}\frac{dV}{dt}.$$

Since I_∞ for the left is identical to I_∞ for the right side of the sample, it is clear that $I_l^{IP,e}+I_l^{IP,h}=I_r^{IP,e}+I_r^{IP,h}$, which is simply the statement that the conductance of the DBRTS, Eqs. (4) and (8), is uniquely defined independent of the two analyses.

The electron and hole charges in the quantum well, Q_w^e and Q_w^h, may recombine to emit light. Hence they are related to the tunneling currents as

$$\frac{dQ_w^e}{dt}=I_l^e(t)-I_r^e(t)-\frac{\mathcal{N}}{\tau}, \tag{11}$$

$$-\frac{dQ_w^h}{dt}=I_r^h(t)-I_l^h(t)-\frac{\mathcal{N}}{\tau}. \tag{12}$$

The terms $\mathcal{N}/\tau$ are due to recombination of electrons and holes, and will be defined later in details in Eq. (16). It has also been studied elsewhere.[4,23] The sign of Eq. (12) originates from our treatment of all charges as electronic charge. If we analyze the quantity $d(Q_w^e+Q_w^h)/dV$, subtracting Eqs. (11) and (12), and making use of Eqs. (5) and (9) and the uniqueness of conductance, we obtain the desired conservation law (10),

$$\begin{aligned}\frac{d}{dV}(Q_w^e+Q_w^h)&=\frac{[I_l^e(t)+I_l^h(t)]-[I_r^e(t)+I_r^h(t)]}{dV/dt}\\&=\frac{[I_l^{OP,e}(t)+I_l^{OP,h}(t)]-[I_r^{OP,e}(t)+I_r^{OP,h}(t)]}{dV/dt}\\&=-\frac{d}{dV}(Q_l+Q_r).\end{aligned}$$

We have then established the fact that our results are independent of which side of the DBRTS one chooses to work with.

B. Linear response

To proceed further from the formal expressions (4) and (5) we consider the situation of a small amplitude ac voltage superimposed to a steady state dc bias,

$$V(t)=V_0+\delta V(t)=V_0+\delta V\sin\,\omega t. \tag{13}$$

Since the hot electron relaxation time[24] is typically less than 10^{-13} s, which is an order of magnitude shorter than the lifetime of electrons and holes in the quantum well,[25] we can define the quasi-Fermi levels at steady state for electrons and holes in the well.[4,17] For frequencies, ω, less than the relaxation rate this is still a valid assumption. Since the quasi-Fermi levels are uniquely determined by the densities of electrons and holes, the tunneling currents are functions of $V(t)$, $Q_w^e(t)$, and $Q_w^h(t)$, at the same time instant, as demonstrated elsewhere.[17] We can then reformulate the differential equations (11) and (12) in the closed form

$$\frac{dQ_w^e}{dt}=I_l^e(V,Q_w^e)-I_r^e(V,Q_w^e)-\frac{1}{\tau}\mathcal{N}(V,Q_w^e,Q_w^h), \tag{14}$$

$$-\frac{dQ_w^h}{dt}=I_r^h(V,Q_w^h)-I_l^h(V,Q_w^h)-\frac{1}{\tau}\mathcal{N}(V,Q_w^e,Q_w^h). \tag{15}$$

We notice that the equations are coupled together by the recombination term $\mathcal{N}/\tau$, which can be written in the compact form[4,23]

$$\frac{\mathcal{N}}{\tau}=\frac{2}{\tau}\int\frac{d^2\vec{k}}{(2\pi)^2}f_e(\vec{k},V,Q_w^e)\,f_h(\vec{k},V,Q_w^h). \tag{16}$$

In our approach the recombination time τ is an experimentally determined parameter. When not otherwise indicated we will use the value $\tau=1$ ns, which is consistent with our assumption of a quasiequilibrium in the well.

With $\delta V/V_0\ll 1$, and in regions where $I_{l/r}(V)$ is fairly linear in an interval δV around V_0, we can safely treat the system in the framework of linear response. In this case the charges in the quantum well can be written as

$$Q_w^e(t)=Q_{w,0}^e+\delta Q_w^e(t),$$

,

$$Q_w^h(t)=Q_{w,0}^e+\delta Q_w^h(t),$$

where $Q_{w,0}^{e/h}$ is the steady-state charge. Under steady state the tunneling currents balance each other, and we have the conditions

$$I_l^e(V_0,Q_{w,0}^e)-I_r^e(V_0,Q_{w,0}^e)=\frac{1}{\tau}\mathcal{N}(V_0,Q_{w,0}^e,Q_{w,0}^h),$$

$$I_r^h(V_0,Q_{w,0}^h)-I_l^h(V_0,Q_{w,0}^h)=\frac{1}{\tau}\mathcal{N}(V_0,Q_{w,0}^e,Q_{w,0}^h).$$

Using these conditions the differential equations (14) and (15) are linearized as

$$\begin{aligned}\frac{d}{dt}\delta Q_w^e=&\left(\left.\frac{\partial(I_l^e-I_r^e)}{\partial V}\right|_{ss}-\frac{1}{\tau}\left.\frac{\partial\mathcal{N}}{\partial V}\right|_{ss}\right)\delta V(t)\\&+\left(\left.\frac{\partial(I_l^e-I_r^e)}{\partial Q_w^e}\right|_{ss}-\frac{1}{\tau}\left.\frac{\partial\mathcal{N}}{\partial Q_w^e}\right|_{ss}\right)\delta Q_w^e(t)\\&-\left(\left.\frac{1}{\tau}\frac{\partial\mathcal{N}}{\partial Q_w^h}\right|_{ss}\right)\delta Q_w^h(t)\\\equiv&A_e\delta V\sin\,\omega t+B_e\delta Q_w^e(t)+C_e\delta Q_w^h(t),\end{aligned} \tag{17}$$

and

$$-\frac{d}{dt}\delta Q_w^h=\left(\left.\frac{\partial(I_r^h-I_l^h)}{\partial V}\right|_{ss}-\frac{1}{\tau}\left.\frac{\partial\mathcal{N}}{\partial V}\right|_{ss}\right)\delta V(t)+\left(\left.\frac{\partial(I_r^h-I_l^h)}{\partial Q_w^h}\right|_{ss}-\frac{1}{\tau}\left.\frac{\partial\mathcal{N}}{\partial Q_w^h}\right|_{ss}\right)\delta Q_w^h(t)-\left(\left.\frac{1}{\tau}\frac{\partial\mathcal{N}}{\partial Q_w^e}\right|_{ss}\right)\delta Q_w^e(t)$$

$$\equiv A_h\delta V\sin\omega t+B_h\delta Q_w^h(t)+C_h\delta Q_w^e(t), \tag{18}$$

where the coefficients $A_{e/h}$, $B_{e/h}$, and $C_{e/h}$ are the partial derivatives evaluated at steady state.

We are interested in the solutions $\delta Q_w^e(t)$ and $\delta Q_w^h(t)$ in response to a periodic ac voltage of frequency ω. Consequently the solutions of the two coupled equations (17) and (18) have the form

$$\delta Q_w^e(t)=\left\{\frac{\delta V}{(\omega^2+C_eC_h)^2+\omega^2(B_e^2+B_h^2)+B_eB_h(B_eB_h-2C_eC_h)}\right\}\{[(A_eB_hC_eC_h+A_hB_eB_hC_e-A_eB_eB_h^2-A_hC_e^2C_h)-\omega^2(A_hC_e+A_eB_e)]\sin\omega t-[(A_eC_eC_h+A_eB_h^2-A_hB_hC_e-A_hB_eC_e)-\omega^2A_e]\omega\cos\omega t\}, \tag{19}$$

for Eq. (17) and

$$-\delta Q_w^h(t)=\left\{\frac{\delta V}{(\omega^2+C_eC_h)^2+\omega^2(B_e^2+B_h^2)+B_eB_h(B_eB_h-2C_eC_h)}\right\}\{[(A_hB_eC_eC_h+A_eB_eB_hC_h-A_hB_e^2B_h-A_eC_eC_h^2)-\omega^2(A_eC_h+A_hB_h)]\sin\omega t-[(A_hC_eC_h+A_hB_e^2-A_eB_eC_h-A_eB_hC_h)-\omega^2A_h]\omega\cos\omega t\}, \tag{20}$$

for Eq. (18).

To obtain the conductance (4) and the susceptance (5) we calculate self-consistently the charge distribution, the tunneling currents, and the recombination current at steady state for all voltages V_0.[4] Within the linear response regime we can then derive dQ_l/dV and the coefficients $A_{e/h}$, $B_{e/h}$, and $C_{e/h}$. Consequently, we obtain $\delta Q_w^e(t)$ and $\delta Q_w^h(t)$ in Eqs. (19) and (20), and calculate the time-dependent tunneling currents $I_l^e(t)$ and $I_l^h(t)$. Separating out the components $I_l^{IP,e/h}(t)$ and $I_l^{OP,e/h}(t)$, we have then obtained all quantities required for calculating the conductance (4) and the susceptance (5).

In our earlier work on the admittance of the unipolar DBRTS (Ref. 17) we identified the capacitive and inductive contributions to the total intrinsic admittance to settle the controversy on this subject. We will here perform a similar analysis for the bipolar DBRTS. In the expression for the susceptance (5) the last part, $\omega dQ_l/dV$, is clearly a regular linear function of frequency, and thus contributes capacitively to the susceptance. The more interesting part of Eq. (5) is $\omega(I_l^{OP,e}+I_l^{OP,h})/(dV/dt)$. From our detailed numerical analysis we find that this is proportional to

$$\frac{\omega+\omega^3}{(\omega^2+C_eC_h)^2+\omega^2(B_e^2+B_h^2)+B_eB_h(B_eB_h-2C_eC_h)}.$$

For the unipolar DBRTS the corresponding expression has the form $\omega/(\omega^2+\Omega^2)$, with an easily identifiable *internal frequency* Ω.[17] Here the internal frequency is not so easy to identify explicitly in terms of the coefficients $B_{e/h}$ and $C_{e/h}$. However, as our numerical results will show, such an internal frequency exists also for the bipolar DBRTS. Let us call it Ω, and then consider the low-frequency limit $\omega\ll\Omega$ and the high-frequency limit $\omega\gg\Omega$.

In the low-frequency limit, $\omega\ll\Omega$, both terms in the expression given above contain odd positive powers of ω and so are regular. Inductance is, however, identified with a singular term diverging as $1/\omega$. Consequently, in the regime of linear response, for low frequencies the susceptance is of a purely capacitive nature. This is exactly the same result as we found for the unipolar DBRTS.[17]

In the high-frequency limit, $\omega\gg\Omega$, the situation is different. We still have the regular part from dQ_l/dV contributing to capacitance. However, the two frequency-dependent terms found from $\omega(I_l^{OP,e}+I_l^{OP,h})/(dV/dt)$ have to be considered more carefully. By expanding the expression in powers of ω, we find that the first term contains odd negative powers of ω with a leading term $1/\omega$.[3] The second term also contains odd negative powers of ω, but with a leading term $1/\omega$. Thus, in the high-frequency limit, we interpret the contribution from $\omega(I_l^{OP,e}+I_l^{OP,h})/(dV/dt)$ as purely inductive.

To conclude our theoretical analysis we will point out that in the numerical work, presented in Sec. III, the conductance is calculated as $G(V,\omega)=G_0+\delta G$, where the steady-state conductance is given by

$$G_0=[I_l^e(V_0,Q_{w,0}^e)+I_l^h(V_0,Q_{w,0}^h)]/V_0$$

and

$$\delta G=[\delta I_l^{IP,e}(t)+\delta I_l^{IP,h}(t)]/\delta V\sin\omega t.$$

III. NUMERICAL RESULTS

The steady-state properties of bipolar DBRT structure have been studied in details in our previous work[4] using a two-band model, by solving eight equations self-consistently: the Poisson equation, two Schrödinger equa-

TABLE I. Structure of sample A (for Figs. 2–7).

Electron emitter	2×10^{18} n^+ $Al_{0.043}Ga_{0.957}As$	400 Å
Spacer	undoped $Al_{0.043}Ga_{0.957}As$	150 Å
Barrier	undoped $Al_{0.3}Ga_{0.7}As$	40 Å
Well	undoped GaAs	50 Å
Barrier	undoped $Al_{0.3}Ga_{0.7}As$	40 Å
Spacer	undoped GaAs	150 Å
Hole emitter	$4\times10^{18}p^+$ GaAs	400 Å

tions, four equations for quantum transport of electrons and holes, and the equation for electron-hole radiative recombination. All physical parameters are calculated from first principles, except the electron-hole recombination time τ, which is treated as an empirical parameter. With proper choices of the geometric structure and the chemical composition of the DBRT diode, its electroluminescence can be optimized. The *I-V* curves of such optimized DBRT LED's exhibit extremely sharp *negative differential resistance* (NDR). As we will show later that the characteristic features of the admittance of a DBRT diode are connected to its NDR, our present numerical studies will be based on those bipolar DBRT structures that have been investigated in Ref. 4.

We have chosen to study two different samples, sample A and sample B, which appear as sample A and sample C in Ref. 4. The structures of the samples are described in Tables I and II, respectively. In sample A the thermally excited electrons and holes are tuned into simultaneous resonant tunneling at bias voltage 1.405 V for $T=300$ K. Sample B reaches the threshold for simultaneous resonant tunneling at bias voltage 1.61 V for $T=10$ K. However, the chemical composition of sample B blocks the electrons and holes from tunneling out of the well because of the large band gaps in the electron and hole emitters. Consequently $I_r^e=I_l^h=0$ for sample B, which is one of the requirements for an optimized RT LED,[4] and which will have strong effect on the admittance of the DBRTS.

Let us first concentrate on sample A. In Fig. 2 we show $\mathrm{Im}(Y)/\omega$ (solid curve) and the conductance G (dashed curve) as functions of bias voltage at the frequency $\omega=10^9$ s^{-1} and temperature $T=300$ K. The kink in the conductance at voltage 1.4 V marks the onset of resonant tunneling. In the NDR region around bias voltage 1.575 V $\mathrm{Im}(Y)/\omega$ exhibits a sharp, almost δ-shaped maximum. Qualitatively this is very similar to what we have found for the unipolar DBRTS.[17]

In Fig. 3 we show $\mathrm{Im}(Y)/\omega$ as function of both bias voltage and frequency at $T=300$ K for sample A. The increase in $\mathrm{Im}(Y)/\omega$ when the sample is tuned into simultaneous

TABLE II. Structure of sample B (for Figs. 8–15).

Electron emitter	2×10^{18} n^+ $Al_{0.11}Ga_{0.89}As$	400 Å
Spacer	undoped $Al_{0.11}Ga_{0.89}As$	50 Å
Barrier	undoped $Al_{0.3}Ga_{0.7}As$	40 Å
Well	undoped GaAs	60 Å
Barrier	undoped $Al_{0.3}Ga_{0.7}As$	40 Å
Spacer	undoped $Al_{0.08}Ga_{0.92}As$	30 Å
Hole emitter	3×10^{18} p^+ $Al_{0.08}Ga_{0.92}As$	400 Å

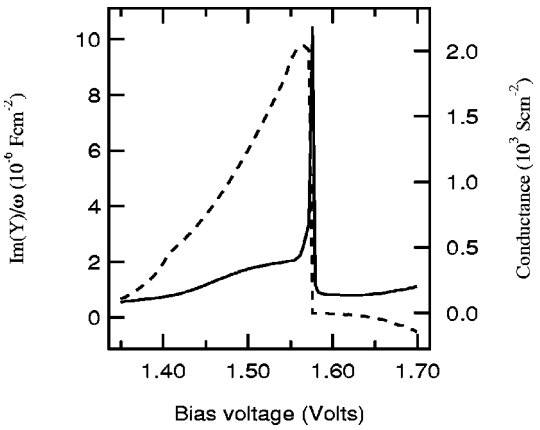

FIG. 2. $\mathrm{Im}(Y)/\omega$ (solid curve) and conductance (dashed curve) for the frequency $\omega=10^9$ s^{-1} as function of voltage at temperature $T=300$ K for sample A.

resonant tunneling is seen as a marked shoulder centered slightly below $\omega=10^9$ s^{-1}, and suggests an internal frequency of sample A slightly below $\omega=10^9$ s^{-1}. This agrees well with the recombination time $\tau=1$ ns, and indicates that the recombination process dominates the frequency response of this DBRTS. To further clarify the frequency response of sample A we have plotted in Fig. 4 $\mathrm{Im}(Y)/\omega$ as function of frequency at bias voltage 1.575 V where $\mathrm{Im}(Y)/\omega$ has its peak value. The peak value $\mathrm{Im}(Y)/\omega=10.8\times10^{-6}$ F cm^{-2} occurs at $\omega=6\times10^8$ s^{-1}, which is recognized as the internal frequency Ω of sample A at 1.575 V and $T=300$ K. In Fig. 4 we also notice that for $\omega<10^7$ $s^{-1}\ll\Omega$ and $\omega>10^{10}$ $s^{-1}\gg\Omega$, $\mathrm{Im}(Y)/\omega$ is frequency independent. This is also seen in Fig. 3.

The conductance of sample A is examined in greater detail in Figs. 5, 6, and 7. In Fig. 5 the solid curve is for the steady-state conductance G_0, the dashed curve for the frequency $\omega=10^6$ s^{-1} and the dash-dotted curve for the fre-

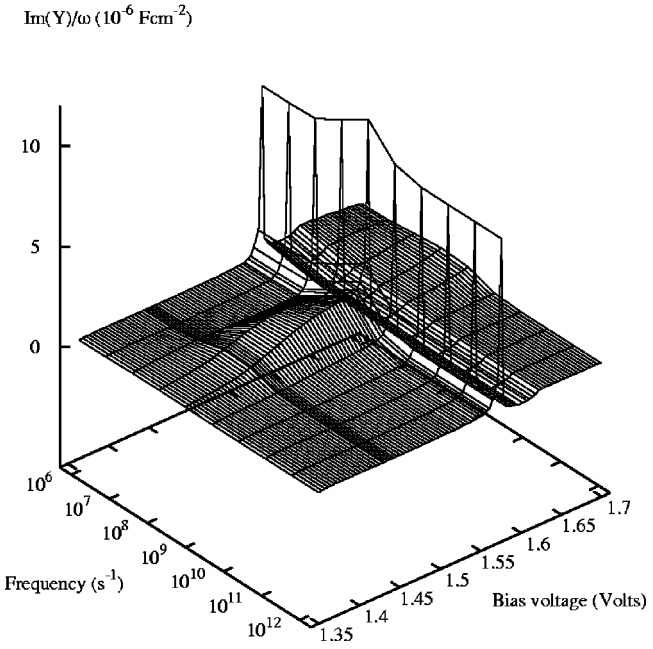

FIG. 3. $\mathrm{Im}(Y)/\omega$ for frequencies $\omega=10^3$ to 10^{12} s^{-1} as function of voltage at temperature $T=300$ K for sample A.

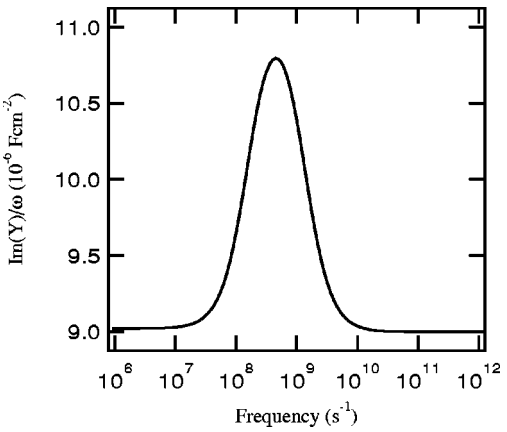

FIG. 4. Frequency dependence of $\mathrm{Im}(Y)/\omega$ at voltage 1.575 V and $T=300$ K for sample A. Under these conditions $\mathrm{Im}(Y)/\omega$ has the peak value.

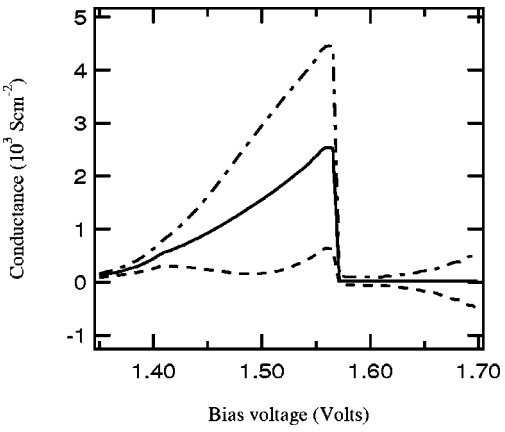

FIG. 5. Conductance-voltage characteristics at steady state (solid curve) and at frequencies $\omega=10^6$ s^{-1} (dashed curve) and 10^{12} s^{-1} (dash-dotted curve) for sample A at temperature $T=300$ K.

quency $\omega=10^{12}$ s^{-1}. The frequency-dependent contribution δG is negative for the low frequency $\omega=10^6$ s$^{-1}\ll\Omega$ and positive for the high frequency $\omega=10^{12}$ s$^{-1}\gg\Omega$. This is similar to what is found in the unipolar DBRTS.[17] In Fig. 6 the conductance is shown as function of both bias voltage and frequency. The behavior of G as function of frequency is clearly very different from that of $\mathrm{Im}(Y)/\omega$ shown in Fig. 3. However, we see that around the internal frequency $\Omega=6\times10^8$ s^{-1} the conductance changes dramatically. This is further clarified in Fig. 7, where we plot the conductance as a function of frequency at bias voltage 1.575 V. Around the internal frequency $\Omega=6\times10^8$ s^{-1} the conductance changes from a low frequency value $G=6.1\times10^2$ S cm^{-2} to a high frequency value $G=4.4\times10^3$ S cm^{-2}. Also this feature is very similar to the behavior found in the unipolar DBRTS.[17]

When electrons and holes can not tunnel out of the quantum well one would expect a much sharper and narrower NDR region and a much lower conductance. In the analysis of Sample B we pursue these questions further. In Fig. 8 $\mathrm{Im}(Y)/\omega$ for sample B is plotted at the low frequency $\omega=10^2$ s^{-1} for the temperature $T=10$ K. The sharp peak at bias voltage 1.678 V coincides with the NDR region, as seen from the conductance shown in Fig. 9. Compared to sample A the δ peak in $\mathrm{Im}(Y)/\omega$ is much sharper and the NDR region is much narrower just as expected. This behavior is seen when comparing Figs. 2, 8, and 9. The large maximum in $\mathrm{Im}(Y)/\omega$ centered at bias voltage 1.595 V has a quite different origin than the δ peak in the NDR region. From our detailed analysis we found that in the bias region where this

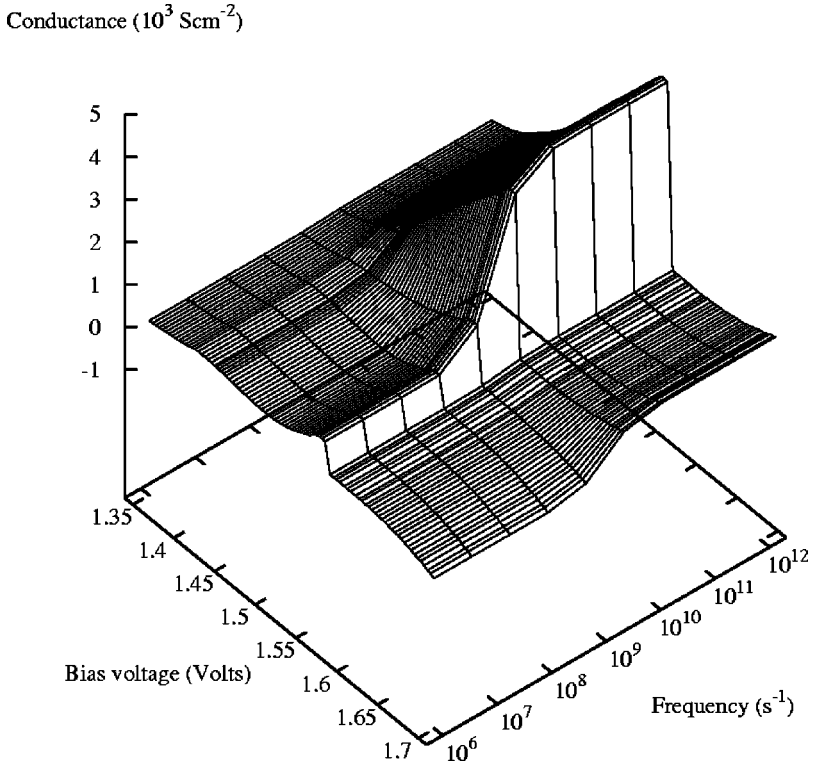

FIG. 6. Conductance-voltage characteristics for frequencies $\omega=10^6$ to 10^{12} s^{-1} for sample A at temperature $T=300$ K.

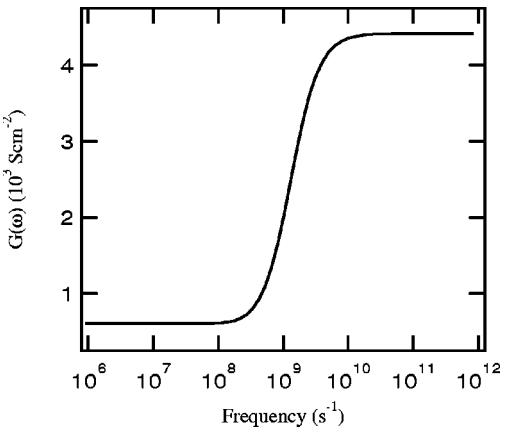

FIG. 7. Frequency dependence of the conductance at voltage 1.575 V and $T=300$ K for sample A. Under these conditions $\mathrm{Im}(Y)/\omega$ has the peak value.

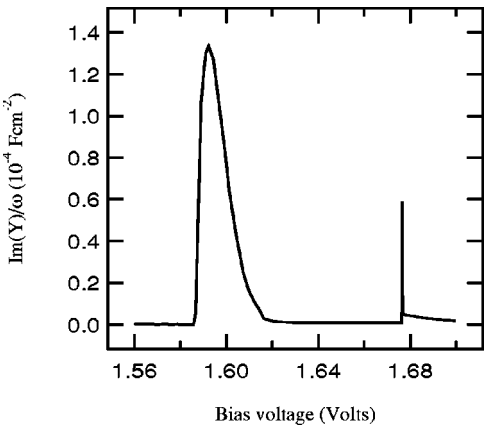

FIG. 8. $\mathrm{Im}(Y)/\omega$ for the frequency $\omega=10^2\ \mathrm{s}^{-1}$ as function of voltage at temperature $T=10$ K for sample B.

maximum occurs we have $I_l^h\neq 0$, but $I_r^e=0$. This means that under such specific conditions the electrons can only tunnel into but not out of the quantum well, while the hole current can flow through the entire sample. The phenomenon resides outside the operational bias voltage region of a RT LED, and is not desirable for an optimized RT LED.[4] However, it has very dramatic consequences for the intrinsic admittance, which we will investigate further in the following.

Our numerical analysis also showed that outside the bias voltage region from 1.57 to 1.64 V we have $I_r^e=I_l^h=0$ in sample B. Furthermore we have found that

$$I_r^e(t)=0\Rightarrow\frac{\partial I_l^e}{\partial V}=\frac{1}{\tau}\frac{\partial\mathcal{N}}{\partial V}\Rightarrow A_e=0$$

and

$$I_l^h(t)=0\Rightarrow\frac{\partial I_r^h}{\partial V}=\frac{1}{\tau}\frac{\partial\mathcal{N}}{\partial V}\Rightarrow A_h=0.$$

All terms in the numerical expressions for $I_l^e(t)$ and $I_l^h(t)$ contain either factors with A_e or factors with A_h. Consequently, when $A_e=A_h=0$ the admittance is frequency independent. This is a very important result for the optimized RT LED. However, it also means that the actual operational bias voltage region of the optimized RT LED is quite uninteresting for further investigation of the frequency response. We therefore concentrate on the frequency dependence of the admittance in the bias voltage region from 1.57 to 1.64 V, where we have the very special situation that only $I_r^e=0$.

In Fig. 10 we show $\mathrm{Im}(Y)/\omega$ in this bias voltage region for frequencies from $\omega=10^2\ \mathrm{s}^{-1}$ to $\omega=10^{12}\ \mathrm{s}^{-1}$. The frequency dependence is clearly very different from that seen in Fig. 3 for sample A. First of all we notice the strong frequency dependence at much lower frequencies than that for sample A, and we can identify an internal frequency approximately $\Omega=10^5\ \mathrm{s}^{-1}$. Since the tunneling into the quantum well has become resonant, or near resonant, in this bias voltage region and we have $I_r^e=0$, we attribute the internal frequency $\Omega=10^5\ \mathrm{s}^{-1}$ to the tunneling of holes out of the well, i.e., to I_l^h. The transparancy of the left barrier for holes in the quantum well is very low because of the large band gap in the electron emitter, and the tunneling process is thus correspondingly slow. Consequently the internal frequency becomes very small. Furthermore, since there is no frequency dependence around $\omega=10^9\ \mathrm{s}^{-1}$, corresponding to the recombination time $\tau=1$ ns, the recombination process is unlikely to be important for the susceptance of sample B.

The conductance of sample B is shown in Fig. 9 for the frequencies $\omega=10^2\ \mathrm{s}^{-1}$ (solid curve), $\omega=10^6\ \mathrm{s}^{-1}$ (dashed curve), $\omega=10^9\ \mathrm{s}^{-1}$ (dotted curve), and $\omega=10^{12}\ \mathrm{s}^{-1}$ (dash-dotted curve). Again we notice that the frequency dependence only resides in the bias voltage range 1.57 to 1.64 V. However we see that in this range the conductance also varies for frequencies $\omega\gg\Omega=10^5\ \mathrm{s}^{-1}$. This is shown clearly in Fig. 11, where we have plotted the conductance for all frequencies from $\omega=10^2\ \mathrm{s}^{-1}$ to $\omega=10^{12}\ \mathrm{s}^{-1}$ in the interesting bias voltage range. This suggests that the recombination process is important for the frequency dependence of the conductance, even though it does not seem to play any role for the susceptance.

When we investigated the steady state properties of the bipolar DBRTS,[4] we analyzed the dynamics of the electroluminescence spectrum by varying the recombination time τ. We follow up this study also for the frequency response of the DBRTS. Let $\Gamma_{e/h}=1/\tau_{e/h}$ be the electron, or hole, tunneling rate through a barrier. Since $\tau_{e/h}$ can be varied by

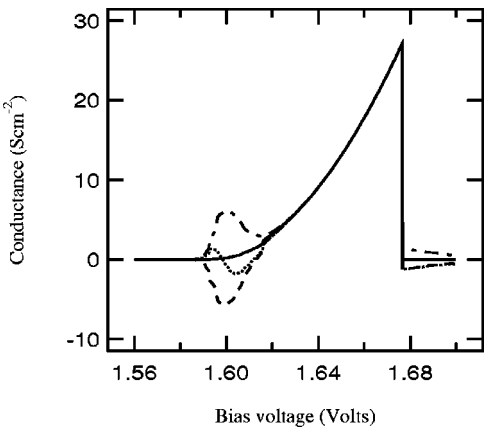

FIG. 9. Conductance-voltage characteristics at frequencies $\omega=10^2\ \mathrm{s}^{-1}$ (solid curve), $\omega=10^6\ \mathrm{s}^{-1}$ (dashed curve), $\omega=10^9\ \mathrm{s}^{-1}$ (dotted curve) and $\omega=10^{12}\ \mathrm{s}^{-1}$ (dash-dotted curve) for sample B at temperature $T=10$ K.

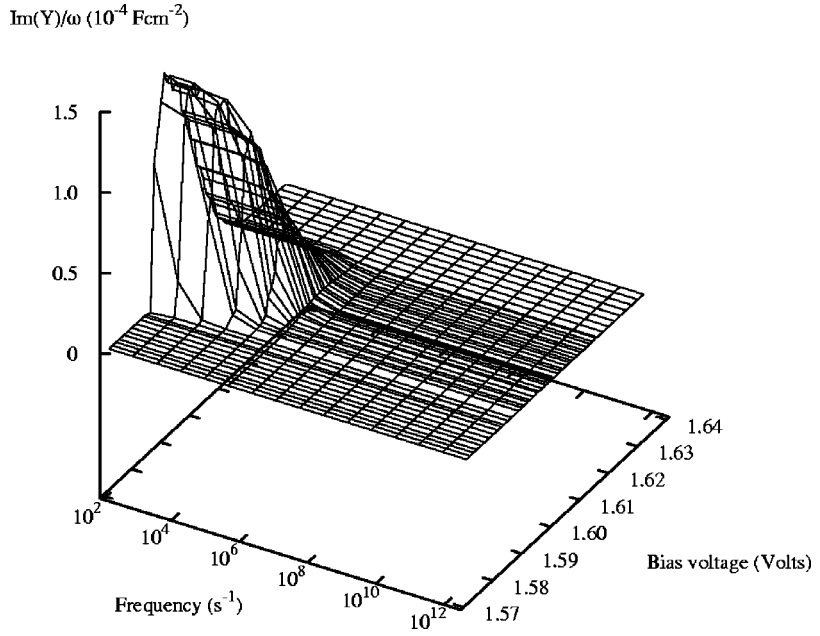

FIG. 10. Im$(Y)/\omega$ for frequencies $\omega=10^2$ to 10^{12} s^{-1} in the voltage range 1.57–1.64 V at temperature $T=10$ K for sample B.

changing the barrier thickness it is interesting to investigate the frequency response when the ratios τ_e/τ and τ_h/τ vary. Instead of changing the structure of the DBRTS we achieve the same goal in a practical way by using τ as a varying parameter. We have then proceeded to do this in the frequency-dependent bias voltage region for sample B. In Fig. 12 we have plotted the peak value of Im$(Y)/\omega$ at bias voltage 1.595 V and at frequency $\omega=10^2$ s^{-1} for recombination times τ in the range 10^{-2} ps to 10^4 ps. The peak value is seen to drop drastically around $\tau=5\times10^{-2}$ ps. We believe the reason for this is that with this high recombination rate the holes in the quantum well are effectively drained through the recombination channel, thus reducing the hole tunneling current I_l^h through the left barrier. Consequently the peak value of Im$(Y)/\omega$ decreases. In Fig. 13 we show Im$(Y)/\omega$ as a function of frequency at the bias voltage 1.595 V for the recombination times $\tau=1$ ns (solid curve) and $\tau=10^{-2}$ ps (dashed curve). Here we also see that the internal frequency Ω is shifted to a slightly higher value.

In Fig. 14 we show the conductance-voltage characteristics at the low frequency $\omega=10^2$ s^{-1} for recombination times ranging from $\tau=10^{-2}$ ps to 10^4 ps. We notice a $1/\tau$ dependence of the magnitude of the conductance, and a tendency of saturation for the shortest recombination time τ

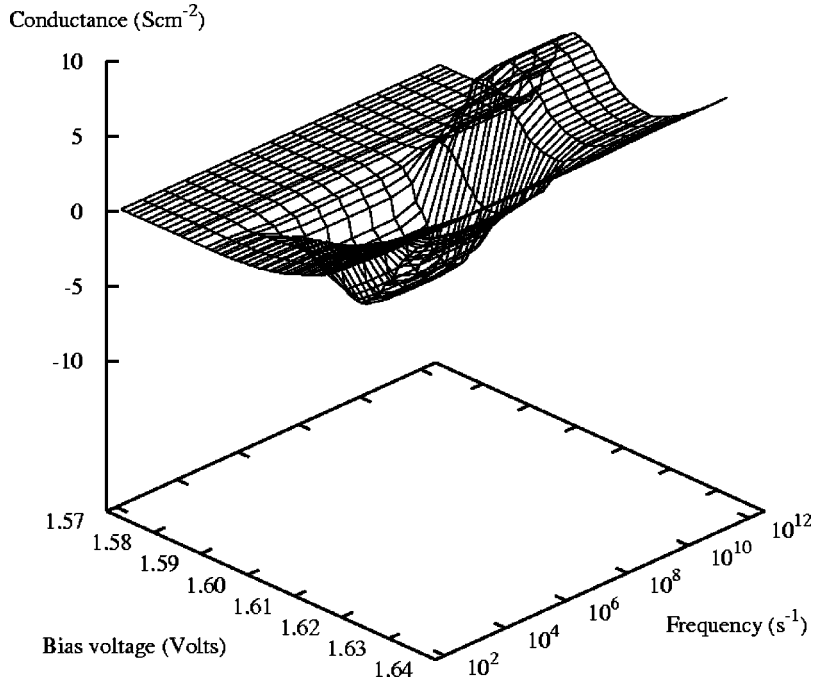

FIG. 11. Conductance-voltage characteristics in the voltage range 1.57–1.64 V for frequencies $\omega=10^2$ to 10^{12} s^{-1} for sample B at temperature $T=10$ K.

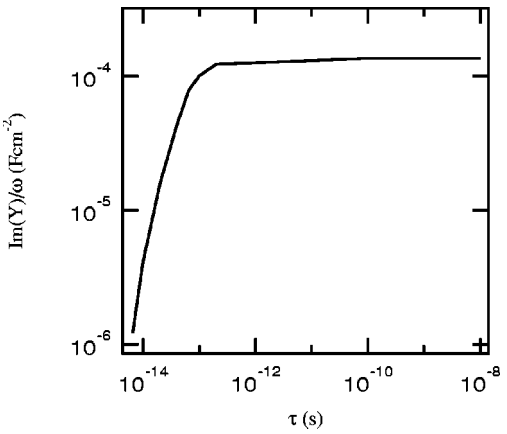

FIG. 12. Im$(Y)/\omega$ at voltage 1.595 V and frequency $\omega = 10^2$ s^{-1} for sample B at temperature $T = 10$ K as a function of the recombination time, which is assumed as a varying parameter.

$= 10^{-2}$ ps. This is reminiscent of what we have earlier found for the steady-state maximum current at bias voltage 1.678 V.[4]

From Fig. 11 we see that the maximum frequency dependence of the conductance of sample B occurs at bias voltage 1.60 V, which is slightly higher than the bias voltage of the peak in Im$(Y)/\omega$. Consequently we have investigated the τ-dependence of the frequency response of the conductance at bias voltage 1.60 V. In Fig. 15 we show the conductance as a function of frequency at this bias voltage for four different recombination times. We notice that there seem to exist two internal frequencies governing the frequency response of the conductance, as already suggested. First there is the lower internal frequency $\Omega = 10^5$ s^{-1}, which we have already identified. This was attributed to the tunneling of holes out of the quantum well, and is seen to be only marginally influenced by varying recombination times τ. The higher internal frequency is, however, completely determined by the recombination time, and we may write it $\Omega_\tau = 1/\tau$. When we analyzed the frequency response of Im$(Y)/\omega$ in Fig. 10, we found no frequency dependence around Ω_τ. Furthermore we see that the overall magnitude of the conductance increases as $1/\tau$, as already seen from

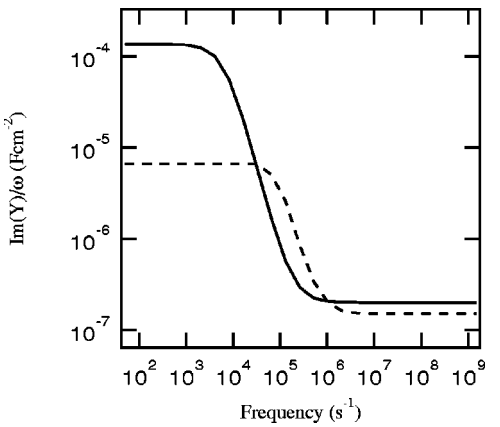

FIG. 13. Frequency dependence of Im$(Y)/\omega$ at voltage 1.595 V and $T = 10$ K for sample B for recombination time $\tau = 10^3$ ps (solid curve) and $\tau = 10^{-2}$ ps (dashed curve). Under these conditions Im$(Y)/\omega$ has a local maximum.

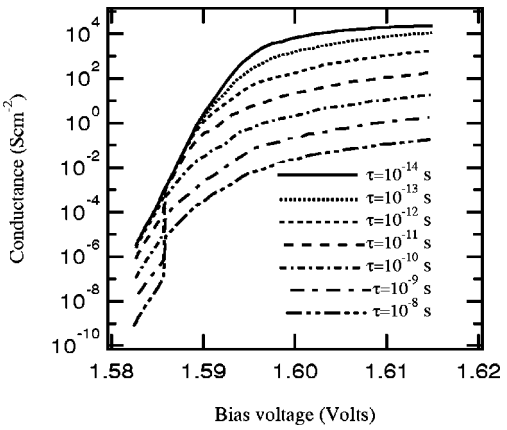

FIG. 14. Conductance-voltage characteristics in the voltage range 1.5825–1.615 V and at the low frequency $\omega = 10^2$ s^{-1} for recombination times $\tau = 10^{-8}$ s to 10^{-14} s for sample B at temperature $T = 10$ K.

Fig. 15, but that the magnitude of the frequency response remains constant down to $\tau = 1$ ps and then even decreases for $\tau = 10^{-2}$ ps. This suggests that the recombination time affects the steady-state conductance and Ω_τ, but has marginal effect on both the susceptance and the magnitude of the frequency response of conductance.

IV. DISCUSSION

In Eqs. (4) and (5) we have provided an exact expression for the total intrinsic admittance of the bipolar DBRTS. To solve the problem numerically we treated the steady-state problem in the Hartree approximation, and then employed the framework of linear response. However, to investigate the response of the bipolar DBRTS to larger ac amplitudes, it would be interesting to proceed beyond the linear response approximation.

Our analysis of the dependence of admittance on recom-

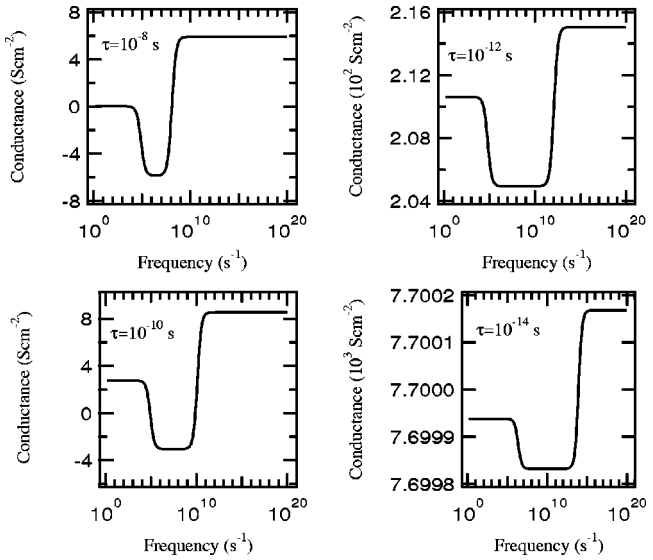

FIG. 15. Frequency dependence of the conductance at voltage 1.60 V and $T = 10$ K for sample B for recombination times $\tau = 10^{-8}$ s to 10^{-14} s.

bination time, in Fig. 12 to Fig. 15, needs a few remarks. Since the hot electron relaxation time[24] is typically less than 10^{-13} s and the tunneling time[25] is around 10^{-12} s, our results for very short recombination times from $\tau = 10^{-12}$ to 10^{-14} s, and for very high frequencies may violate the validity of our theory. However, the results remain interesting as a guide to identify the different mechanisms which govern the frequency response of the bipolar DBRTS, and also to indicate what happens when the ratios τ_e/τ and τ_h/τ vary from very small to very large.

[1] C. van Hoof, J. Genoe, R. Mertens, G. Borghs, and E. Goovaerts, Appl. Phys. Lett. **60**, 77 (1992).

[2] C. R. H. White, H. B. Evans, L. Eaves, P. M. Martin, M. Henini, G. Hill, and M. A. Pate, Phys. Rev. B **45**, 9513 (1992).

[3] O. Kuhn, D. K. Maude, J. C. Portal, M. Henini, L. Eaves, G. Hill, and M. Pate, Solid-State Electron. **37**, 843 (1994).

[4] A. Kindlihagen, K. A. Chao, and M. Willander, Semicond. Sci. Technol. **12**, 535 (1997).

[5] S. Luryi, Appl. Phys. Lett. **52**, 501 (1988).

[6] T. Jungwirth and L. Smrčka, Phys. Rev. B **51**, 10 181 (1995).

[7] M. E. Lazzouni and L. J. Sham, Phys. Rev. B **48**, 8948 (1993).

[8] R. C. Ashoori, H. L. Stormer, J. S. Weiner, L. N. Pfeiffer, S. J. Pearton, K. W. Baldwin, and K. W. West, Phys. Rev. Lett. **68**, 3088 (1992).

[9] K. Fobelets, R. Vounckx, J. Genoe, G. Borghs, H. Grönqvist, and L. Lundgren, Appl. Phys. Lett. **64**, 2523 (1994).

[10] Y. Zhang, Y. Li, D. Jiang, X. Yang, and P. Zhang, Appl. Phys. Lett. **64**, 3416 (1994).

[11] J. Genoe, C. Van Hoof, W. Van Roy, J. H. Smet, K. Fobelets, R. P. Mertens, and G. Borghs, IEEE Trans. Electron Devices **ED-38**, 2006 (1991).

[12] Y. Hu and S. Stapleton, Appl. Phys. Lett. **58**, 167 (1991).

[13] S. Luryi, Appl. Phys. Lett. **59**, 2335 (1991).

[14] T. Wei and S. Stapleton, J. Appl. Phys. **76**, 1287 (1994).

[15] Y. Fu and S. C. Dudley, Phys. Rev. Lett. **70**, 65 (1993).

[16] N. Zou, M. Willander, and K. A. Chao, Phys. Rev. B **50**, 4980 (1994).

[17] A. Kindlihagen, A. G. Malshukov, K. A. Chao, and M. Willander, preceding paper, Phys. Rev. B **58**, 10 603 (1998).

[18] W. R. Frensley, Appl. Phys. Lett. **51**, 448 (1987).

[19] L. Y. Chen and C. S. Ting, Phys. Rev. Lett. **64**, 3159 (1990).

[20] H. C. Liu, Phys. Rev. B **43**, 12 538 (1991).

[21] W-R. Liou and P. Roblin, IEEE Trans. Electron Devices **41**, 1098 (1994).

[22] C. L. Fernando and W. R. Frensley, Phys. Rev. B **52**, 5092 (1995).

[23] G. D. Mahan and L. E. Oliveira, Phys. Rev. B **44**, 3150 (1991).

[24] C. H. Yang, J. M. Carlson-Swindle, S. A. Lyon, and J. M. Worlock, Phys. Rev. Lett. **55**, 2359 (1985).

[25] T. C. L. G. Sollner, W. D. Goodhue, P. E. Tannenwald, C. D. Parker, and D. D. Peck, Appl. Phys. Lett. **43**, 588 (1983).